AIAA 2003-3450

Hypersonic Transition Research in the Boeing/AFOSR Mach-6 Quiet Tunnel

Steven P. Schneider, Craig Skoch,
Shann Rufer, and Erick Swanson
School of Aeronautics and Astronautics
Purdue University
West Lafayette, IN 47907-1282 USA

33rd Fluid Dynamics Conference
23–26 June 2003
Orlando, FL

AIAA Paper 2003-3450, 33rd AIAA Fluid Dynamics Conference, Orlando, Florida, 23-26 June 2003

Hypersonic Transition Research in the Boeing/AFOSR Mach-6 Quiet Tunnel

Steven P. Schneider*, Craig Skoch†, Shann Rufer‡, and Erick Swanson§
School of Aeronautics and Astronautics
Purdue University
West Lafayette, IN 47907-1282

Abstract

A Mach-6 Ludwieg tube is being developed for high Reynolds number quiet-flow operation. The model-support centerbody had been causing upstream separation when the nozzle-wall boundary layers became laminar at low pressures. The centerbody has now been removed, resulting in attached Mach 5.7 quiet flow below 8 psia total pressure. Pitot measurements show that low-noise flow begins at the same 8 psia, from halfway down the nozzle to near the nozzle exit. Thus, transition in the nozzle-wall boundary layer is apparently bypassing the usual linear instability processes. Measurements of the static pressure on the diffuser walls show large fluctuation when the nozzle-wall boundary layer is laminar, probably due to upstream propagation of bleed-slot jet noise from the diffuser. Finally, initial oil-flow images show the development of crossflow vortices on a sharp cone at angle of attack, and hot-wire measurements show initial evidence of instability waves on a sharp cone at zero angle of attack.

Introduction

Hypersonic Laminar-Turbulent Transition

Laminar-turbulent transition in hypersonic boundary layers is important for prediction and control of heat transfer, skin friction, and other boundary layer properties. However, the mechanisms leading to transition are still poorly understood. Applications hindered by this lack of understanding include reusable launch vehicles such as the X-33 [1], high-speed interceptor missiles [2], hypersonic cruise vehicles [3], and ballistic reentry vehicles [4].

Many transition experiments have been carried out in conventional ground-testing facilities over the past 50 years. However, these experiments are contaminated by the high levels of noise that radiate from the turbulent boundary layers normally present on the wind tunnel walls [5]. These noise levels, typically 0.5-1% of the mean, are an order of magnitude larger than those observed in flight [6, 7]. These high noise levels can cause transition to occur an order of magnitude earlier than in flight [5, 7]. In addition, the mechanisms of transition operational in small-disturbance environments can be changed or bypassed altogether in high-noise environments; these changes in the mechanisms change the parametric trends in transition [6].

Development of Quiet-Flow Wind Tunnels

Only in the last two decades have low-noise supersonic wind tunnels been developed [5, 8]. This development has been difficult, since the test-section wall boundary-layers must be kept laminar in order to avoid high levels of eddy-Mach-wave acoustic radiation from the normally-present turbulent boundary layers. A Mach 3.5 tunnel was the first to be successfully developed at NASA Langley [9]. Langley then developed a Mach 6 quiet nozzle, which was used as a starting point for the new Purdue nozzle [10, 11]. Unfortunately, this nozzle was removed from service, and an effort towards developing a Mach 8 quiet tunnel was unsuccessful. The new Purdue Mach-6 quiet flow Ludwieg tube is the only operational hypersonic quiet tunnel in the world, at least until the old Langley Mach-6 nozzle is brought back online.

*Associate Professor. Associate Fellow, AIAA.
†Research Assistant. Student Member, AIAA.
‡Research Assistant. Student Member, AIAA.
§Research Assistant. Student Member, AIAA.

Background of the Boeing/AFOSR Mach-6 Quiet Tunnel

A Mach-4 Ludwieg tube was developed at Purdue in 1992-1994 [12]. Quiet flow was achieved at low Reynolds numbers, and the facility was used for development of instrumentation and for measurements of instability waves under quiet-flow conditions [13, 14, 15]. However, the low quiet Reynolds number and the small 4-inch test section imposed severe limitations.

A hypersonic facility that remains quiet to higher Reynolds numbers is needed. The low operating costs of the Mach-4 tunnel had to be maintained. Operation at Mach 6 was selected, since this is high enough for the hypersonic 2nd-mode instability to be dominant under cold-wall conditions, and high enough to observe hypersonic roughness-insensitivity effects, yet low enough that the required stagnation temperatures do not add dramatically to cost and difficulty of operation. Beginning with Ref. [16], a number of AIAA papers have reported on the design, fabrication, and shakedown, on the development of instrumentation, and on progress towards achieving quiet flow.

Ref. [17] summarized these earlier papers, and reported on initial quiet flow achieved at low Reynolds numbers with the 6th bleed-slot design, and also on initial measurements with temperature-sensitive paints and hot wires. Ref. [18] reported a detailed review of the literature for transition on blunt cones and the generic scramjet forebody, along with temperature-sensitive-paints results on the forebody, the results of the 7th bleed-slot throat geometry, and the results of polishing the downstream portion of the Mach-6 nozzle. Recent measurements on the scramjet forebody are reported in Reference [19].

The Boeing/AFOSR Mach-6 Quiet Tunnel

Quiet facilities require low levels of noise in the inviscid flow entering the nozzle through the throat, and laminar boundary layers on the nozzle walls. These features make the noise level in quiet facilities an order of magnitude lower than in conventional facilities. To reach these low noise levels, conventional blow-down facilities must be extensively modified. Requirements include a 1 micron particle filter, a highly polished nozzle with bleed slots for the contraction-wall boundary layer, and a large settling chamber with screens and sintered-mesh plates for noise-reduction [5]. To reach these low noise levels in an affordable way, the Purdue facility has been designed as a Ludwieg tube [12]. A Ludwieg tube is a long pipe with a converging-diverging nozzle on the end, from which flow exits into the nozzle, test section, and second throat (Figure 1). A diaphragm is placed downstream of the test section. When the diaphragm bursts, an expansion wave travels upstream through the test section into the driver tube. Since the flow remains quiet after the wave reflects from the contraction, sufficient vacuum can extend the useful runtime to many cycles of expansion-wave reflection, during which the pressure drops quasi-statically.

Figure 2 shows the nozzle. The region of useful quiet flow lies between the characteristics marking the onset of uniform flow, and the characteristics marking the upstream boundary of acoustic radiation from the onset of turbulence in the nozzle-wall boundary layer. Quiet flow has not yet been achieved except at very low Reynolds numbers, so the acoustic-radiation characteristics are not shown. A 7.5-deg. sharp cone is also drawn on the figure. The rectangles are drawn on the nozzle at the location of window openings, all but one of which are presently filled with blank metal inserts. Images of the tunnel are available at `http://roger.ecn.purdue.edu/~aae519/BAM6QT-Mach-6-tunnel/`, along with earlier papers and other documentation.

Status of Quiet-Flow Performance

Although the tunnel has been operational since April 2001, it is not yet quiet at high Reynolds number. The following subsections describe recent efforts towards improving quiet flow performance.

Second-Throat Model-Support Centerbody

As discussed on p. 19 of Ref. [18], the nozzle-wall boundary layers appeared to become laminar at about 8 psia total pressure; but when they became laminar they appeared to separate, reducing the freestream flow area and lowering the Mach number. It was thought that the model-support/second-throat centerbody (see Ref. [20]) might be causing the upstream separation through a shock/boundary-layer interaction. Although it is not often reported, experimentalists have long known that an impinging shock can cause laminar boundary layer separation more than 50 boundary-layer thicknesses upstream [21, p. 344]. In addition, NASA Langley has observed the onset of transition well upstream on a flared cone, when the nozzle exit shock impinged on the downstream end of the cone (Steve Wilkinson,

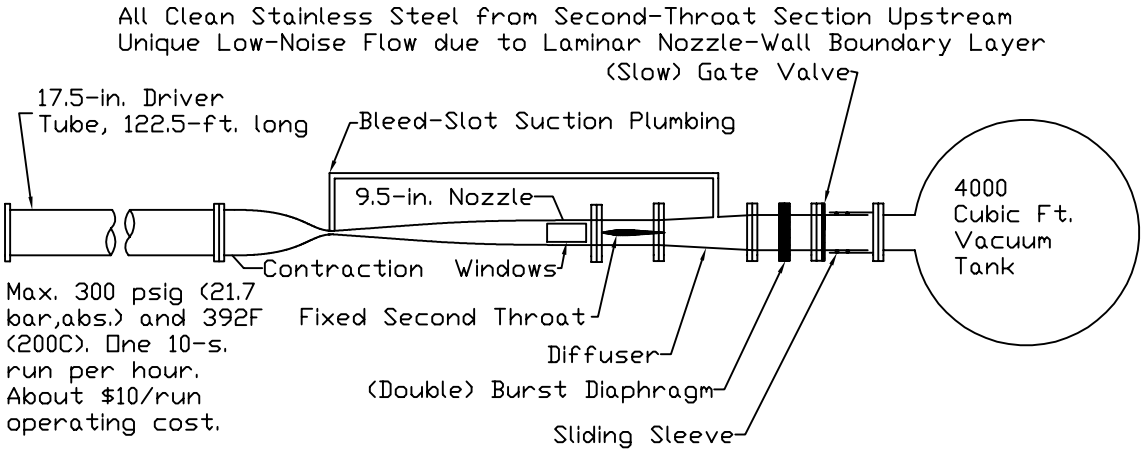

Figure 1: Schematic of Boeing/AFOSR Mach-6 Quiet Tunnel

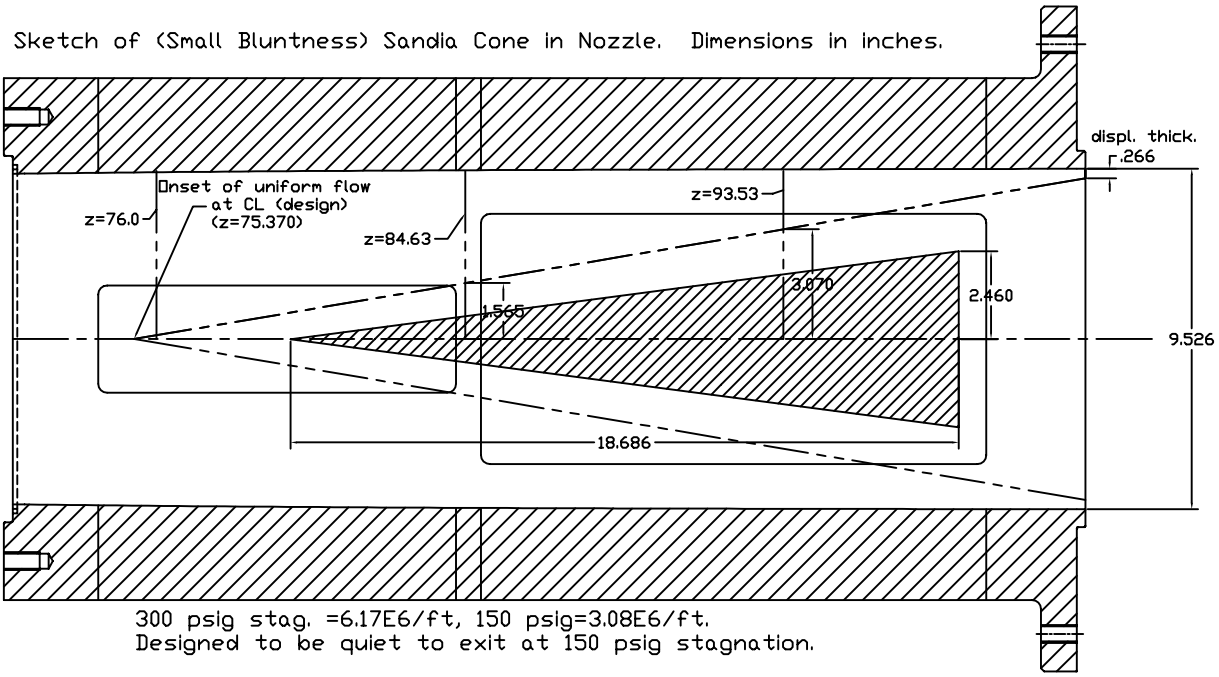

Figure 2: Schematic of Mach-6 Quiet Nozzle with Model

private communication, Jan. 2003). Thus, transition can also be induced well upstream of a shock impingement point. Following the appearance of Ref. [18], tufts were applied to the nozzle wall in the region just forward of the exit. When the pressure dropped low enough for the boundary layer to become laminar, the tufts fluctuated wildly, indicating boundary-layer separation.

It was then decided to remove the second-throat centerbody to enable measurements in a clear tunnel. The tunnel then has a straight circular duct downstream of the nozzle, all the way to the conical subsonic diffuser (into which the bleed-slot-throat air is ducted, see Ref. [20] and Fig. 1). There is no second throat to fix the location of any discrete downstream recompression.

The contraction-entrance Kulite that measures the driver tube pressure failed before doing the runs without the second-throat centerbody. For these new runs previous contraction data were used to estimate the pressure drop in the driver tube during the run. This might not be accurate if the pressure drop changed when the centerbody was removed. The contraction-entrance Kulite has been replaced, and future runs will determine if the pressure drop has changed.

Effect of Removing the Second-Throat Centerbody

The double-wedge centerbody was removed, and new pitot measurements were made in the same location, on the centerline at $z = 84.3$ inches downstream of the throat. Figures 3 and 4 compare the mean Mach number and RMS pitot fluctuations with the previous data taken in the same location with the centerbody present. All data were acquired with a XCQ-062-15A Kulite on a Tektronix 7104 digital scope in High-Res mode at a sampling frequency of 200 kHz. The driver tube temperature in all cases was 160 deg. C. The atmospheric-pressure dewpoint for the new runs was about $-25°C$, compared to $-30°C$ for the winter 2002 runs with the centerbody present. The data are again averaged over 0.1-sec. intervals. The plots include 4 runs with the centerbody removed: 3 from $P_d = 14.4 \pm 0.1$ psia, and one from $P_d = 10.0$ psia, where P_d is the initial driver pressure. The plots also include 5 earlier runs with the centerbody present, with $P_d = 14.2, 14.1, 10.0, 9.8$, and 8.0 psia.

Fig. 3 shows that the mean Mach number now remains near 5.6 as the pressure drops, whereas with the centerbody present it rose and then fell dramatically. The nozzle-wall boundary-layer separation caused by the centerbody apparently caused the sud-

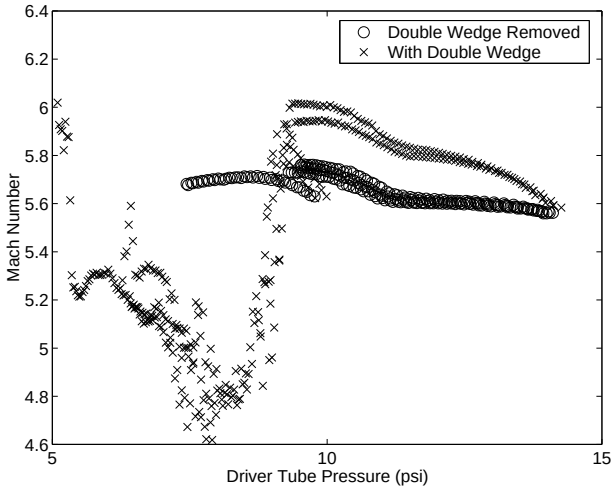

Figure 3: Effect of Centerbody on Upstream Mach Number

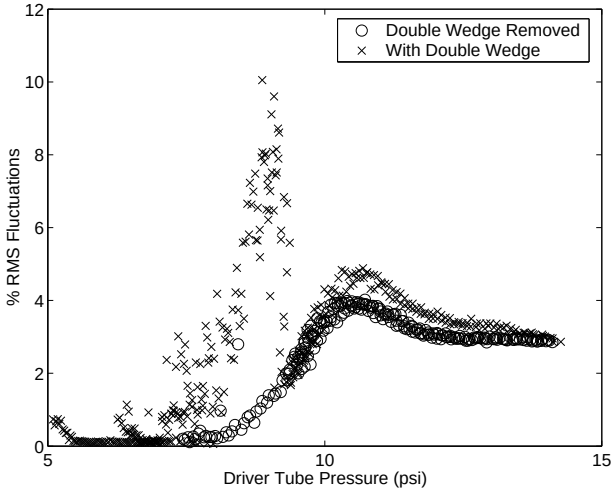

Figure 4: Effect of Centerbody on Upstream Pitot Fluctuations

den fall in Mach number for stagnation pressures below about 8 psia. This fall is no longer present with the centerbody removed, and there is no evidence of separation. With the centerbody double-wedge present, the Mach number rose faster for driver pressures between 14 and 9 psi; the cause of this rise and of the difference is unknown. It is possible that the discrepancy in Mach numbers between the cases is caused by errors in the estimation of the stagnation pressure drop during the run. For the runs with the double-wedge removed, there is a discrepancy between the initial Mach number for the 10-psia initial-pressure run and the final Mach number for the 14.4 psia initial-pressure run; this discrepancy might also be caused by errors in estimating the stagnation-pressure drop.

Fig. 4 shows the RMS fluctuations in the two cases. With the centerbody present, the noise rose dramatically when separation began, and then fell at very low pressures under the separated boundary layer (an interesting effect). In the unseparated flow with the centerbody removed, the noise falls smoothly to low levels at about 8 psia as the boundary layer drops laminar.

Pitot Measurements of Upstream Noise

The nozzle was designed using e^N theory following earlier work at Langley [16, 22, 23]; transition occurs much earlier than was predicted.

To better understand the transition on the nozzle wall, a 33-inch-long pitot-probe shaft was fabricated. This enabled measuring the fluctuations well forward on the nozzle centerline. These measurements were made with the centerbody removed. The 3/4-in.-dia. shaft is supported by a strut centered at $z = 76.421$ inches downstream of the throat. This strut mounts in a forward window-blank insert that was built for Roger Kimmel of AFRL/VA. The shaft is tapered on the front, ending in a XCQ-062-15A Kulite pressure transducer. The transducer tip can be placed at $z = 45.03, 51.03, 57.03, 63.03$, or 69.03 inches, within 1/32 inch of the centerline. For reference, the end of the nozzle is at $z = 101.975$ inches, and the end of the curved part is at $z = 101.734$ in. The nozzle wall angle at the inflection point is 4.00 deg., which is probably the smallest value ever used, since a long nozzle was expected to reduce growth of the Görtler instability [16]. The nozzle has a radial flow section, which begins at $z = 1.31$ in. where the inviscid nozzle wall radius is 0.691 in. Radial flow ends at $z = 23.63$ in., where the inviscid radius is 2.25 in.

Fig. 5 shows the inviscid Mach number computed along the centerline of the nozzle [24]. As far upstream as $z \simeq 55$ in., the inviscid Mach number has dropped only to 5.8, from the exit value of 6.0 (reached first at $z = 75.13$.) This is because the nozzle is so long, with such a gradual change in area. At $z = 45$ inches, halfway down the nozzle, the Mach number from the inviscid computation is already 5.5. Fig. 6 shows the nozzle contour and the right-running characteristics, along which noise is radiated from the nozzle wall to the centerline. These characteristics were computed by the inviscid nozzle-design code [24], but should be reasonable accurate when the boundary layer is thin. The nozzle coordinates were computed by adding a displacement-thickness correction for a laminar boundary layer at a total pressure of 150 psia. This correction amounted to a quarter inch at the exit; at present operating conditions, the boundary layers are thicker than this. The characteristic that reaches the centerline at about $z = 45$ inches originates on the wall at about $z = 29$ inches, where the inviscid radius is 2.7 inches and the local Mach number is 4.6. This acoustic origin is 5-1/2 inches downstream of the end of the radial flow region.

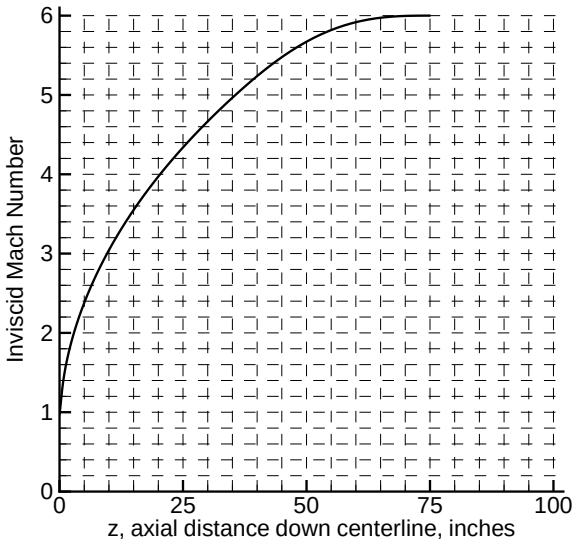

Figure 5: Inviscid Mach Number on the Nozzle Centerline

This then provides some background for comparison to the measurements. Fig. 7 shows Mach number measurements on the centerline for various probe locations. The horizontal axis shows the instantaneous total pressure, averaged over 0.1 sec. intervals as the driver-tube pressure drops. For the aft stations, the Mach number is in the range of 5.6

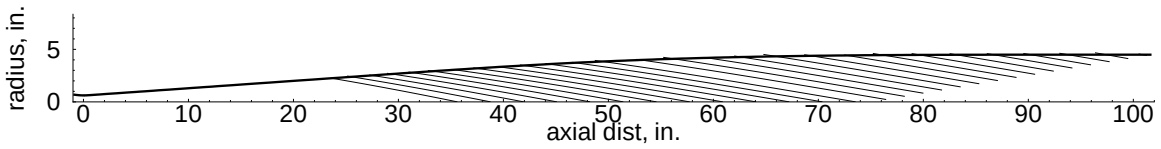

Figure 6: Inviscid Characteristics in the Quiet Nozzle

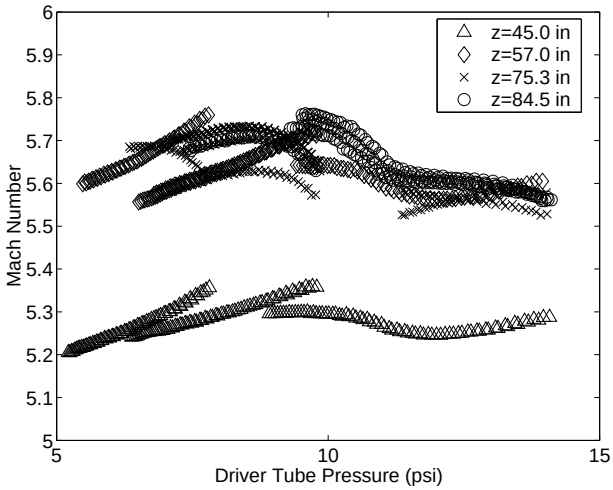

Figure 7: Mach Number in the Quiet Nozzle

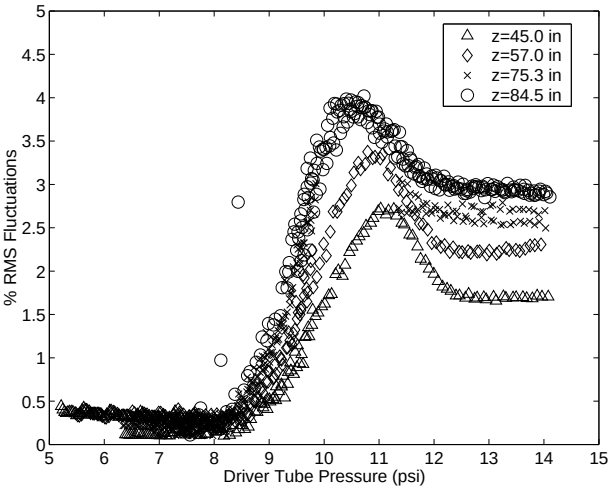

Figure 8: Pitot Fluctuations in the Quiet Nozzle

to 5.7, not far below the design value of 6.0, considering the thick boundary layers present at these low pressures. For the forward station at $z = 45$ inches, the Mach number is noticeably lower, at about 5.3, which also compares reasonably well to the computed value of about 5.5. It is not yet clear why the traces don't repeat more precisely; one possibility is again a mis-estimation of the stagnation pressure drop during the run.

Fig. 8 shows the RMS pitot fluctuations normalized by the mean, at the four stations. During the run, the pressure in the driver tube drops about 40%. Initial driver pressures shown here are 14.37 ± 0.09 psia for 7 traces, 10.05 ± 0.06 psia for 8 traces, and 8.00 ± 0.02 psia for 3 traces. The noise level is somewhat lower at the upstream stations. However, Fig. 8 shows very clearly that the noise level drops dramatically at nearly the same pressures at all streamwise stations. Below about 12 psia, the noise rises, as the turbulent boundary layer drops intermittently laminar, and the passage of turbulent spots radiates high levels of noise. Then below about 8 psia, the flow drops quiet, with a laminar boundary layer, although not in all cases below the nominal quiet-tunnel value of 0.1%. This is possibly due in part to limited signal-noise ratio. Since these effects are nearly independent of streamwise location, it appears that some effect is bypassing the normal linear-instability processes on the nozzle wall.

Throttling the Bleed-Slot Flow to the Diffuser

The flow from the throat-region bleed-slot suction to the diffuser (Fig. 1) was throttled by varying the setting of the ball valves on the plumbing. The figures in this section were all obtained at initial driver pressures of 10.065 ± 0.030 psia. The driver tube temperature was $160°C$. The probe was on the centerline at $z = 75.3$ in. The double-wedge model-support centerbody was removed for these runs. The data were taken on a Tektronix 7104 scope in High-Res mode at a sampling frequency of 200kHz, yielding perhaps 12 bits of resolution. Fig. 9 shows Pitot traces for various throttling settings of the bleed-slot valves. As the bleeds are throttled, less massflow goes through the bleed system, reducing the pressure rise in the vacuum system and increasing the run-time from about 6 sec. to nearly 9 sec. Fig. 10 shows pressures in the suction plenum during these runs. Once the bleed valves are less than half open, the pressure ratio is insufficient to establish sonic flow in the bleed slots.

Fig. 11 shows the Pitot fluctuations for the same

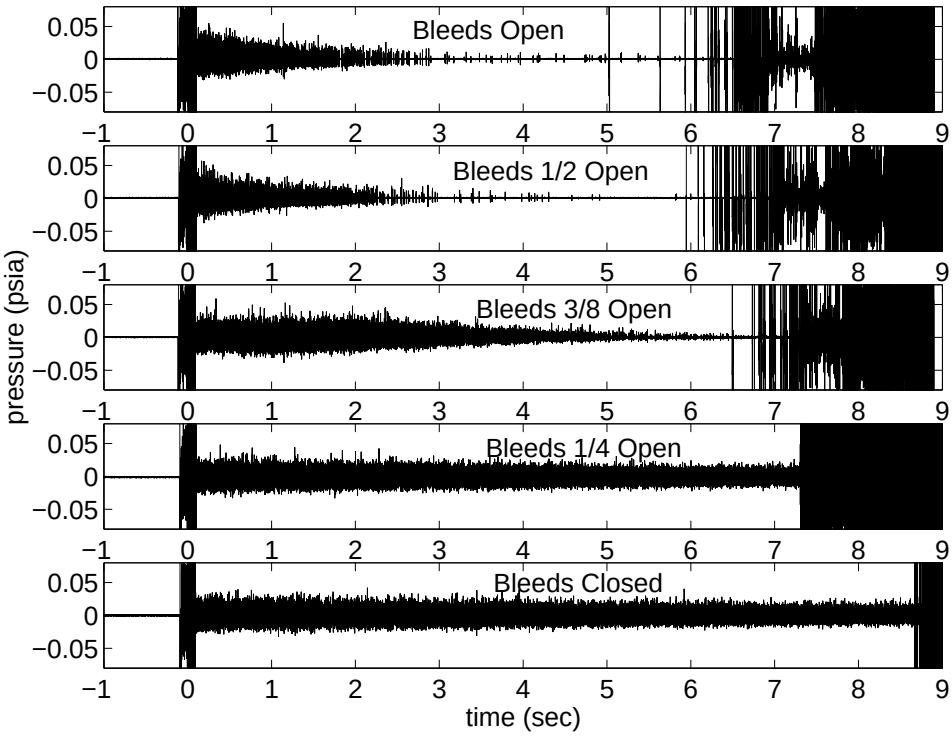

Figure 11: Pitot Fluctuations with Throttled Bleeds

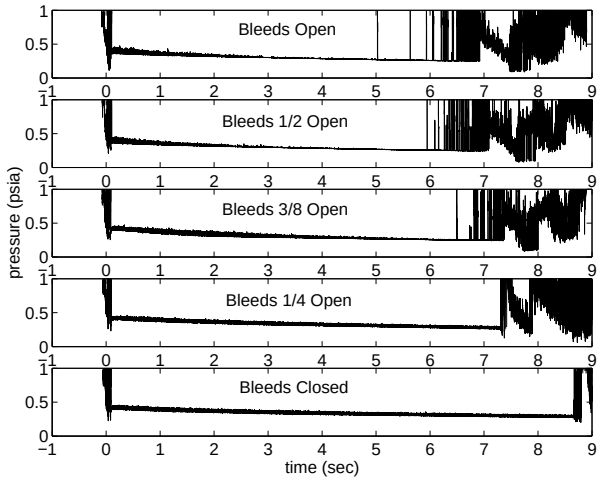

Figure 9: Pitot Traces with Throttled Bleeds

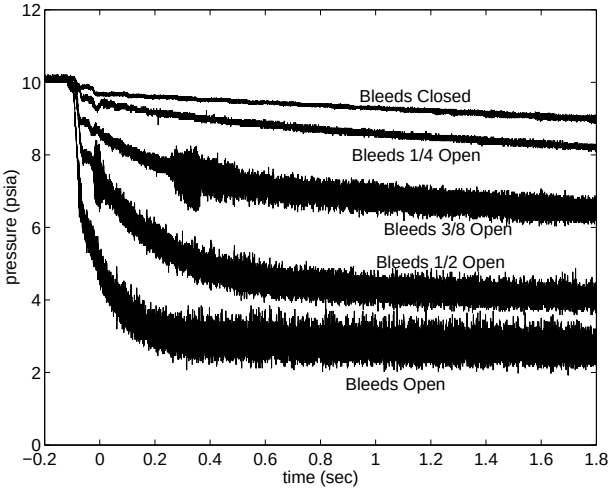

Figure 10: Pressures in the Suction Plenum with Throttled Bleeds

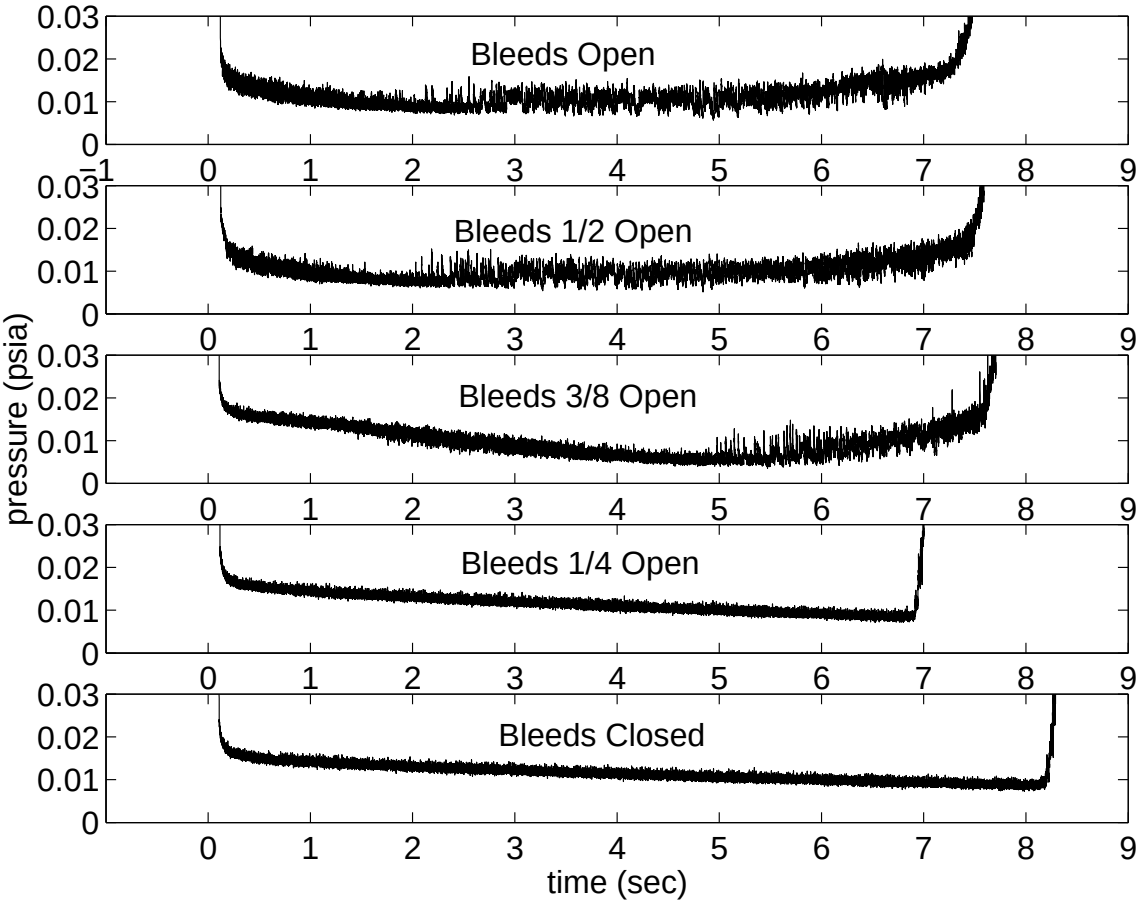

Figure 12: Diffuser Static Pressures with Throttled Bleeds

cases. With the bleeds fully open, the fluctuations start to drop out at about 3 sec., as the driver pressure and unit Reynolds number drops. Similar results are seen with the bleeds half open, while with 3/8-open bleeds a small amount of low-noise flow may appear at about 6 sec. near the end of the run. With 1/4-open or fully-closed bleeds, the flow remains noisy for the full run. This observation is consistent with Fig. 10; the flow through the bleed slot must be sonic to achieve laminar nozzle-wall boundary layers and low-noise flow.

An XCQ-062-15A stopped Kulite pressure transducer was also flush-mounted on the diffuser wall, just downstream of the nozzle exit at $z = 104.850$. The azimuthal location is 45-deg. to the right of the lower side, looking downstream; note that this is aft of the pitot sensor. This sensor has a full-scale range of 15 psia, so it is not very accurate at the static pressure (0.063% of stagnation pressure at Mach 6). However, it gives useful indications. Fig. 12 shows the results for the same 5 runs shown in Figs. 9 and 11. The run with open bleeds shows the noise rising noticeably at about 2-1/2 sec., at about the same time that the noise drops out in Fig. 11. The results with half-open bleeds are similar. With 3/8-open bleeds, the noise rises at about 5 sec., at roughly the same time that the noise starts to drop out on the pitot fluctuations. When the pitot signal shows that the nozzle-wall boundary layer is starting to drop laminar, the diffuser signal shows that noise starts to become evident. With the bleeds 1/4 open or fully closed, and a turbulent nozzle-wall boundary layer, the higher noise is never seen in the diffuser entrance.

Fig. 13 shows a detail of the diffuser fluctuations for a small part of the fully-open and fully-closed runs. The open-valve peak-to-peak fluctuations are about 0.007 psia in this segment, about 2/3 of the mean of about 0.010 to 0.011 psia. The mean is above the Mach-6 static pressure of about 0.008 psia, perhaps due to systematic errors, or perhaps to some pressure recovery upstream of the transducer. The fluctuations are large compared to the mean when the bleeds are open at low pressures, much larger than when the bleeds are closed. Fig. 14 shows uncalibrated spectra at the same conditions, for the bleeds open (upper spectra) and closed (lower). Some 60 Hz noise is evident, along with a large decrease in low-frequency noise when the bleeds are closed.

The data suggests that the jets of bleed air entering the diffuser cause large unsteady fluctuations well upstream at the diffuser entrance. Since these

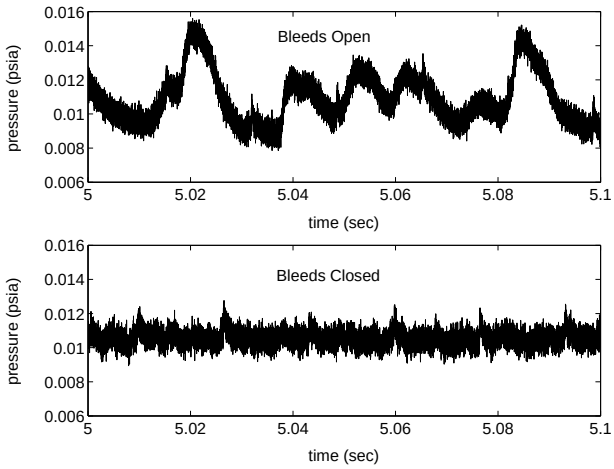

Figure 13: Detail of Diffuser Pressures with Throttled Bleeds

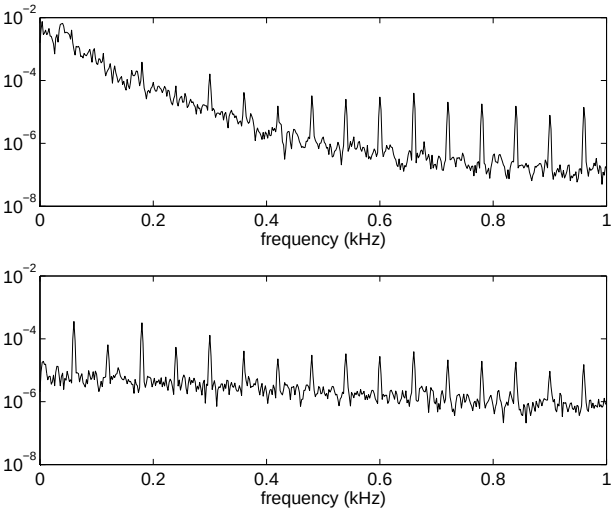

Figure 14: Spectra of Diffuser Pressures with Throttled Bleeds

fluctuations decrease when the nozzle-wall boundary layer is turbulent, it seems possible that they might be feeding upstream and tripping the boundary layer. A fast-opening valve and plumbing are being installed to bypass the bleed air directly to the vacuum tank, rather than into the diffuser. It is hoped that this change will contribute to achieving more quiet flow.

Summary of Quiet-Flow Development Issues

Possible causes of the early transition on the nozzle wall include:

1. Fluctuations generated at the nozzle throat due to problems with the bleed-slot flow. Although several designs have produced similar results, this possibility still cannot be ruled out. A computational analysis is needed, similar to the work underway at ONERA [25].

2. A nozzle-wall temperature distribution that decreases much more rapidly downstream than was initially expected. However, computations suggest this effect should be minor, and there is no evidence to suggest it could cause transition in the way observed.

3. A 0.001-0.002-inch ($Re_k < 12$) rearward-facing step at the downstream end of the electroform [26]. Here, Re_k is a roughness Reynolds number based on the height of the peak roughness, and the conditions in a smooth-wall boundary layer at the roughness height. However, this step was dramatically reduced by the fall 2002 polishing, without noticeable effect [18].

4. Insufficient polish on the downstream nozzle sections (although $Re_k < 12$). However, the fall 2002 polish had no noticeable effect.

5. Noise in the driver tube that doesn't show up in the low-noise pressure measurements made on the contraction wall. This is to be addressed by new measurements planned for the contraction entrance flow.

6. Some fundamental problem with the use of a very long nozzle which is not captured by the e^N analysis. This seems unlikely, since transition now seems to flash forward along the whole downstream half of the nozzle at about the same pressure.

7. Noise propagated upstream from the diffuser section. The original diffuser centerbody apparently caused separation in the nozzle-wall boundary layer when it began to drop laminar. Upstream propagation of disturbances remains a concern, even with the model support removed, due to the jets of air from the bleed-slot suction that enter the diffuser downstream. These jets are to be removed by plumbing this bleed air directly to the vacuum tank; this work should be completed by the end of the summer.

8. Flaws in the throat-region polish. A small bump was felt on the bleed lip during the last assembly in late 2002, and it is possible that this bump is tripping transition. The bleed lip polish is to be reworked sometime late this summer.

9. Leaks in the low-pressure sections that cause jets of air into the nozzle, tripping the boundary layer. Although testing with soap films under pressure have not shown such leaks, small leaks may still be present. More sensitive leak tests with a helium sniffer are to be carried out.

10. Vibrations of the bleed lip, introducing disturbances that trip the flow. The tunnel vibrates when the flow starts up, but although these vibrations can clearly be felt, they seem to damp within a second or two. However, the onset of transition seems to occur at the same pressure, regardless of whether this pressure is at the beginning or the end of a run, making this cause seem less likely. The Mach-4 tunnel did not have this problem, but it did not use throat suction either, and the bleed lips may be more sensitive to vibration, particularly in the transverse direction. More vibration measurements are to be made.

11. Earlier, air could flow from the circulation heater upstream of the driver tube through the supply piping and into the driver tube, during a run. This air would flow when the expansion wave from the driver tube reflected from the upstream end, lowering the pressure. Since it is known from the Mach-4 tunnel that a jet of air entering the driver tube during the run will preclude quiet flow, an electronically controlled valve was added to the supply pipe at the entrance to the driver tube, so this source of air could be shut off. However, tests carried out so far indicate that this valve has no effect on quiet flow.

Progress in Tunnel Operations

Sealing Issues

Reliable sealing is a critical issue for quiet facilities in particular, since small leaks upstream of the throat can cause noise, and small leaks in the nozzle section can trip the nozzle-wall boundary layer. Silicone O-rings have been used to seal between the sections of the 304 stainless steel driver tube. The original O-rings were Parker silicone S604-70 material. These are rated for indefinite service at about $450°F$ (e.g., p. 2-30 of the 2001 Parker O-ring handbook). The driver tube has not been heated above $360°F$, and is mostly maintained at $320°F$, yet these O-rings have been routinely failing after serving for periods of the order of a year. The O-rings crumble and stick to the (once clean) stainless-steel flanges; after some time they begin to leak. In May 2003 the driver tube was cooled for a sensitive leak test using a helium sniffer; immediately upon cooling, all the O-ring joints started to leak, and the usual deterioration was found. This is after a couple of years of operation, during which the driver tube is maintained at about $320°F$ for most of the time, exposed only to air that is mostly dry.

Teflon encapsulated silicone O-rings are now being used. One of these has been used for about a year in the joint between the first and second sections of the contraction. These O-rings do not seem to decompose and they do not stick to the stainless steel, although they do take a set after awhile, losing resiliency and conforming to the rectangular groove shape. If the Teflon-encapsulated rings also fail too frequently, the new Kalrez (Dupont) or Parafluor (Parker) materials may be tried, although these are very expensive in the 2-465 size used on the 18-inch driver tube.

Time Required for Driver Air to Reach Equilibrium

A series of runs was performed to find the optimal settling time between filling the tunnel with air and bursting the diaphragms. When new heated air is added to the hot driver tube, the settling time allows the air and pipe to reach equilibrium, so the air has a nearly uniform temperature [27]. Until now, a settling time of 30 minutes had been used, but the best value was unknown. An optimum was sought, since this time is a large factor in determining the number of runs which can be completed in a day.

Two sets of runs were conducted - the first set compared settling times of 10, 30, and 60 minutes, and the second (done two weeks after the first) compared settling times of 1, 10, 30, 60 and 240 minutes.

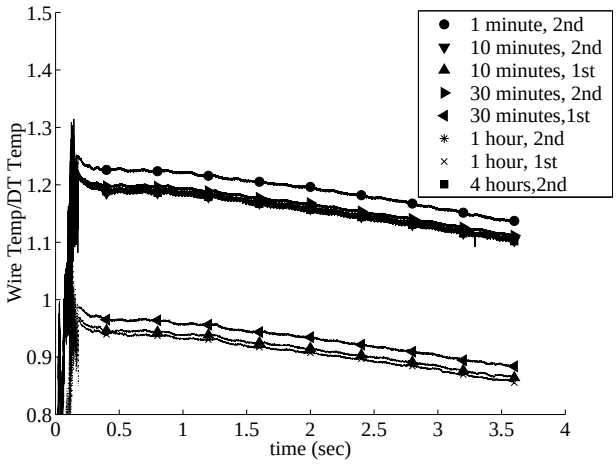

Figure 15: Cold-Wire Measurements of Stagnation Temperature for Various Settling Times

The hot wire used during these runs was Pt-10% Rh, with a diameter of 0.00015 inches. The length-to-diameter ratio was approximately 131, the cold resistance was 10 ohms, and the wire survived a total of more than 50 runs. A 2.5 mA constant-current anemometer was used to sense the wire resistance, with the resistance being converted to temperature using an oven calibration. A calibration of wire temperature vs. stagnation temperature and Reynolds number has not yet been carried out (cp. Ref. [28]). The driver-tube pressure was approximately 45 psia and the driver-tube temperature was 433K. The commercial circulation heater (which heats the air entering the driver tube) was set to heat to 438K, and was normally enabled 20-30 sec. before the air began to flow into the driver tube. If the tunnel has not been operated for several hours, the circulation heater is cold, and is enabled perhaps 45 seconds before air starts to flow. The control system of the circulation heater sets the heater power so that the outgoing air is at the set temperature, as measured with a thermocouple; however, this system only works after the air flow is turned on.

The results of these runs are shown in Figure 15. The vertical axis is the wire temperature normalized by the initial driver-tube temperature, and the horizontal axis is the time after the start of the run. There is a significant offset between the data for the first set of runs and that of the second set. Although the reason for this is not clear, it could be due, in part, to a change in the cold resistance of the wire caused by stress [29, pp. 22-23].

It appears from this figure that all of the curves of the second set of runs fall on top of each other,

except for the 1 minute settling time. The first set of runs shows an offset in the data with a 30 minute wait time, but this may fall within the repeatability of the tunnel, or be due to wire strain-hardening effects Any settling period longer than 1 minute may be sufficient, but the the 10 minute settling period is clearly sufficient, and much shorter than the 30 minutes presently used. Therefore, a 10 minute settling period is to be used for future runs in the Mach 6 tunnel. Further cold-wire runs are to be carried out to better determine the stagnation-temperature variation during the tunnel runs, along with repeatability.

Crossflow Effects on Blunt Cones at Angle of Attack

When a cone is pitched to angle of attack, a pressure gradient exists laterally around the cone, driving fluid from the windward to the leeward side. The pressure gradient has a larger effect on the low-momentum fluid near the wall, turning it more than the fluid at the edge of the boundary layer and creating a component of velocity perpendicular to the edge streamline velocity. This is the crossflow component [30]. The crossflow velocity profile reaches a maximum somewhere in the middle of the boundary layer. Since the velocity in the boundary layer decreases toward the wall due to viscous effects, the imposed pressure gradient (constant across the layer at Mach 6) has a greater turning effect on the flow, and the crossflow velocity initially increases toward the wall. However, the strong viscous forces near the wall due to the no-slip condition drive all velocity components to zero, thus decreasing the crossflow velocity to zero in the lower part of the boundary layer. Thus, an inflection point is found in the crossflow profile, typically somewhat above the maximum [31]. This inflection point causes an inviscid crossflow instability that may result in a series of corotating vortices in the boundary layer [31, 32], approximately aligned with the edge streamline.

The crossflow instability may be a dominant cause of transition on pitched re-entry vehicles. Therefore, an understanding of the mechanism of crossflow-induced transition is crucial to the design of such vehicles. A research program has been initiated at Purdue University to study the crossflow mechanism as well as to produce a data base of transition locations on pitched cones in the Mach 6 tunnel. Temperature sensitive paint and oil-flow techniques are being used to visualize crossflow vortices.

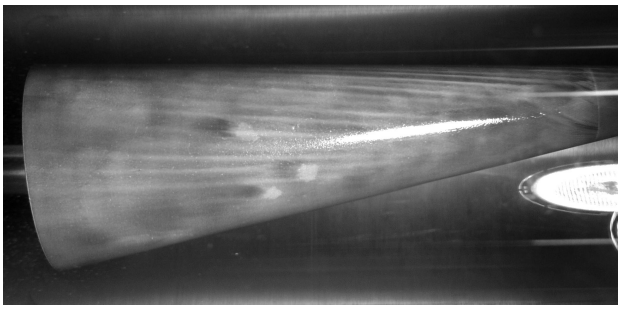

Figure 16: Oil-Flow Image of Crossflow Vortices on a Cone at Angle of Attack

Early oil-flow experiments are described below. Hot-wires will be used to measure boundary layer profiles and instability waves. Hot-film arrays will be used to measure transition location. The effects of roughness on crossflow-induced transition will also be studied. Various computer codes will be used to predict boundary layer profiles and instability wave growth. The experimental results will be used to verify the calculations. The Lubard-Helliwell Hypersonic Viscous Shock Layer code [33] is currently being modified to predict streamline and vortex angles on pitched sharp cones using the method of Adams [34]. These computations will be verified by comparison to the experimental results of McDevitt and Mellenthin [35], who measured vortex angles on the 90-deg. ray of pitched cones at various freestream conditions. The code will then be used to predict vortex angles for comparison to results in the Purdue Mach 6 tunnel.

The oil-flow technique has been used to visualize crossflow vortices on a 7-deg. half-angle sharp cone with a two-inch base radius at 6-deg. angle-of-attack in the Purdue Mach-6 Tunnel. Figure 16 illustrates these vortices at a Reynolds number of 3×10^6/ft and freestream Mach number of 6. The driver-tube temperature was $160°C$ and the cone was near room temperature. The cone is pitched in the vertical plane, with the camera view from the side. Zinc oxide artist paint was mixed into Dow Corning 200 Fluid (100 cs or 200 cs viscosity) and painted on the cone just before insertion into the tunnel. The cone surface was painted with black spray paint so that the white oil mixture would show up against the surface. The run was made as soon as the tunnel was brought up to pressure. The standard 30-minute settling period before starting the tunnel run was skipped due to concerns over the oil dripping off the cone. The camera was set up to take four sequential pictures during the run, triggered by hand. The im-

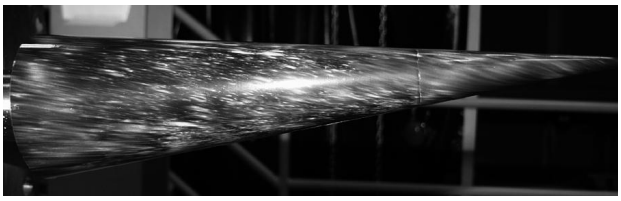

Figure 17: Oil-Flow Image of Streamlines on a Cone at Angle of Attack

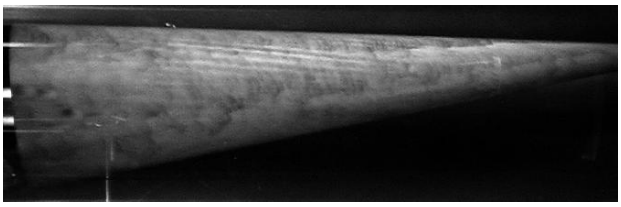

Figure 18: Second Oil-Flow Image of Crossflow Vortices

age in Figure 16 is the fourth of these pictures. The time between images was not controlled. Dow Corning 200 fluid, 100 cs, was used for the run illustrated in Figure 16.

An expansion wave passes through the test section to start the run. The oil begins to flow as the flow starts over the cone. After a short time (not yet determined), flow features such as vortices appear in the oil. The vortices are visualized as the gray regions between the bright white streaks in Figure 16. The vortices sweep away the oil underneath them, resulting in a series of peaks (bright white concentrations of oil) to either side and valleys (grayer areas where there is less oil) underneath the vortex [34, p. 4]. The vortices appear to curve in a similar fashion to the streamlines (Figure 17, discussed below), although there appears to be the expected slight angle between the streamline and vortex directions. This might indicate that the orientation of the vortices changes with the crossflow distribution, as is expected of the orientation of the instability waves [34]. Fig. 17 was taken after the run, with the cone removed from the nozzle.

The streamlines in Figure 17 were visualized by spritzing the white oil paint onto the cone. The brush was dipped into the paint and the bristles were flicked, spraying dots of paint on the cone. During the run, the flow dragged these dots along, producing the streaks seen in the image. This image was taken after the run had ended, so there is some effect due to tunnel shut down. As the tunnel run ends, a shock wave travels forward through the test section. This shock causes the oil on the cone to move somewhat.

The vortices in Figure 16 are similar to those seen in the TSP picture reproduced in Figure 26 of Ref. [18]. The TSP technique visualized the higher heat transfer due to the turbulent boundary layer on the rear of the cone, as well as the vortices produced by the two roughness elements on the bottom half of the cone. It can be seen from Figure 26 of Ref. [18] that the heat transfer due to the turbulent boundary layer is about the same as that due to the vortices, obscuring them from view on the rear of the cone. The oil flow technique was expected to be more sensitive to the coherent, large-scale motions of the vortices rather than the random turbulent fluctuations on the rear of the cone. Thus, the oil flow technique is a better method for visualizing the development of the crossflow vortices on the rear of the cone, where the boundary layer is expected to be turbulent. Vortices were also observed on the front of the cone, where none were seen with the TSP. It is possible that the paint layer used in those tests was not sensitive enough to detect the weaker portions of the vortices on the front of the cone, possibly since the insulating layer was too thin.

Figure 18 shows an image of the cone at $Re = 2.63 \times 10^6$/ft and Mach 6. This image was taken from video shot during the run with a Sony MiniDV camcorder. The same 7-deg. cone is again at a 6-deg. angle of attack. A series of vortices can be seen in the central section of the top half of the cone. These vortices are qualitatively similar to the streaks seen in TSP images at the same condition.

The updated Lubard-Helliwell VSL code will be used to predict the vortex angles in the oil flow and TSP images presented here and in Ref. [18]. Initially, the predictions will be made only for vortices on the 90-deg. ray, since the cone would have to be digitally 'unwrapped' to measure the angles on other rays. An algorithm that processes the images in this way will be developed or found so that vortex angle predictions can be tested on the rest of the cone.

Hot-Wire Measurements on Sharp Cone

Hot-wire measurement work continues, with initial development being performed on a 7 degree half-angle sharp cone at zero angle of attack. The hot wire was placed 11.7 inches axially downstream from the tip of the cone. The wire is Pt-10%Rh, with a diameter of 0.00015 inches. The cold resistance of the wire was 11.5 ohms and the length-to-diameter

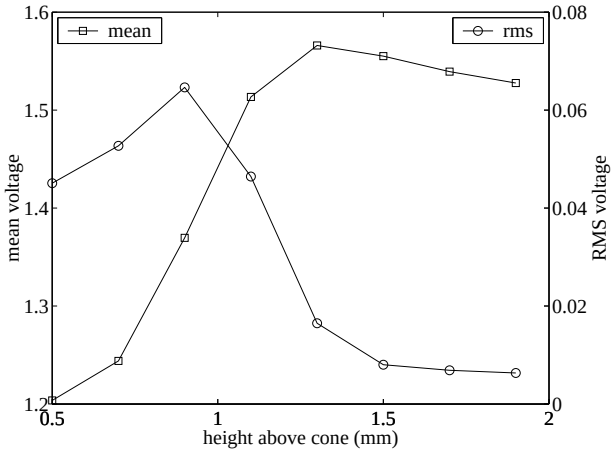

Figure 19: Boundary-Layer Profile on Sharp Cone at $P_d = 95$ psia

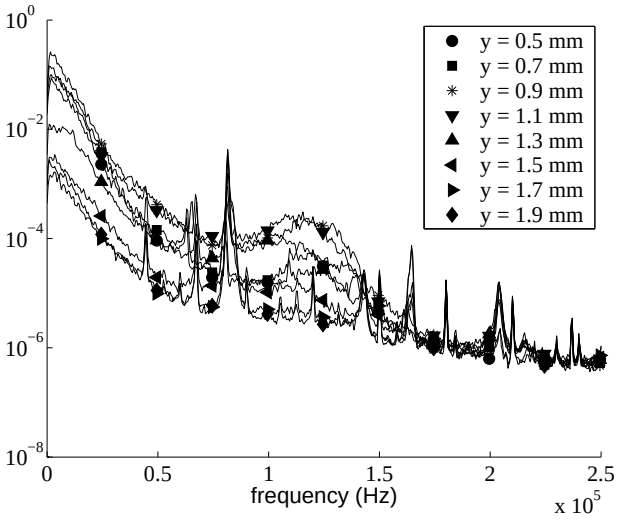

Figure 20: Uncalibrated Spectra from Boundary-Layer Profile on Sharp Cone at 95 psia

ratio was approximately 140. A single wire of this type has survived more than 50 runs at varying driver-tube pressures up to 140 psia. A TSI IFA-100 constant-temperature anemometer was used, with a one-to-one bridge. The overheat ratio of 1.8 makes the wire primarily sensitive to mass-flow fluctuations; calibrations are planned. The square-wave frequency response was 225 kHz, as measured in still air at ambient pressure. The anemometer output was sampled at 1 MHz for 2 seconds in Hi-Res mode using a Tektronix 7104 digital oscilloscope. The driver temperature was set to 433K for these runs. The automated vertical traverse is used to obtain a boundary-layer profile during a single run [18].

The hot wire is initially positioned at approximately 0.5mm above the cone. The wire is stationary until 0.32 seconds after flow startup, at which point it is moved away from the cone by 0.2 mm in 0.127 seconds. The wire remains at this location for 0.1 seconds and then the process is repeated for 20 steps, placing the wire 4.5 mm from the surface at the end of the run. During the 0.1 second interval when the wire location is fixed, the data can be processed to obtain the mean and rms voltage. Fig. 19 shows a typical profile, performed at a driver-tube pressure of $P_d = 95$ psia, similar to Fig. 28 in Ref. [18]. The mean voltage increases as the wire moves away from the wall and the boundary-layer mass-flow increases. A slight decrease is observed above about 1.3 mm from the wall. This drop may be due to the slow stagnation-pressure drop that occurs as gas flows from the driver tube; no correction for this effect has yet been implemented. The RMS peaks near the boundary-layer edge, as expected.

Fig. 20 show uncalibrated power spectra obtained at the various wire positions. The usual low-frequency noise is observed, as is typical of facilities operating under turbulent nozzle-wall boundary layers. A number of steep spikes are observed, possibly caused by vibrations or electrical interference. The broad peak near 120 kHz appears to be instability waves, since it reaches a maximum near 1.1 mm, near the edge of the boundary layer. It is curious that broad peak in the spectra reaches a maximum farther from the wall than the RMS does. Fig. 21 shows a typical segment of the time-trace record, taken at 1.3 mm above the wall, where the broad peak is near a maximum. Irregular waves can be seen in the 2 ms segment, with roughly 23-29 peaks visible, roughly corresponding to the expected frequency.

Similar runs were made at five different pressures, in an attempt to clarify the presence of instability waves. The probe was held in the same axial position. For each pressure, a traverse similar to Fig. 19 was made, and the peak rms value was located. The peak heights were 1.5, 1.1, 0.9, 0.7, and 0.5 mm for stagnation pressures of 45, 75, 95, 115, and 135 psia. Thus, the peak height decreases with decreasing boundary-layer thickness, as expected. The 0.2-mm increments in the locations of profile measurements can be modified in the future to improve resolution.

Spectra at each of these peak RMS heights are plotted in Fig. 22. A broad peak appears near 100kHz at 75 psia driver pressure (freestream

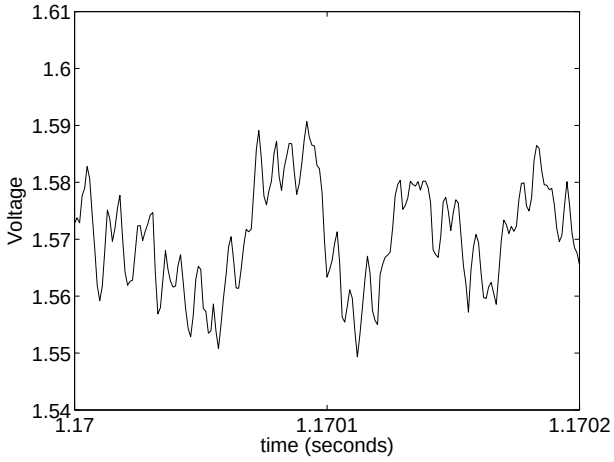

Figure 21: Time-Trace from Boundary-Layer Profile on Sharp Cone

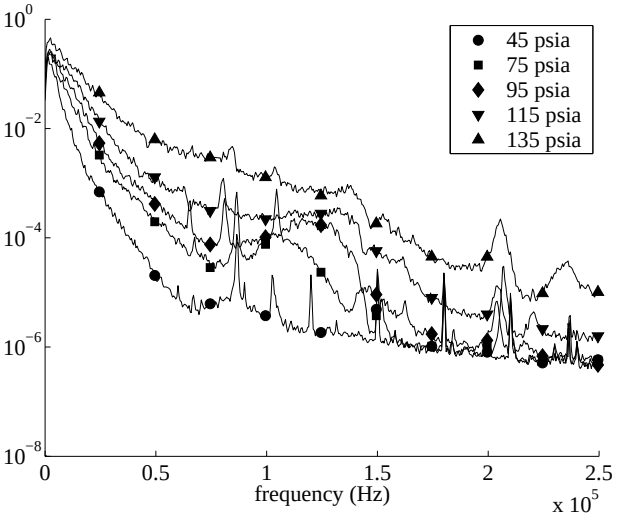

Figure 22: Effect of Stagnation Pressure on Sharp-Cone Fluctuation Spectra

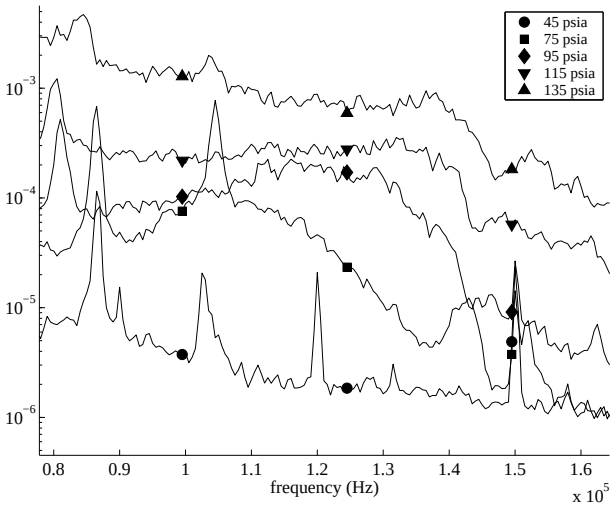

Figure 23: Detail of Sharp-Cone Fluctuation Spectra

$Re_\infty \simeq 1.8 \times 10^6$/ft), and increases in amplitude and frequency through 95 psia ($Re_\infty \simeq 2.3 \times 10^6$/ft) and 115 psia ($Re_\infty \simeq 2.8 \times 10^6$/ft). At 135 psia ($Re_\infty \simeq 3.3 \times 10^6$/ft) it appears to wash out with increasing levels of low-frequency noise, perhaps due to the onset of turbulence. Transition was earlier apparent in temperature-paints measurements on a 7-deg. sharp cone at zero angle of attack at $Re_\infty \simeq 3 \times 10^6$/ft, consistent with this observation [18, Fig. 25]. At 45 psia ($Re_\infty \simeq 1.1 \times 10^6$/ft) no clear peak is evident, perhaps because the instabilities have not yet amplified above the background noise.

Fig. 23 shows a detail of the broad peak. With a freestream velocity of about 870 m/s (near edge velocity U_e for a 7-deg. cone) and a boundary layer thickness δ of about 1.3 mm at 95 psia (Fig. 19), one would expect second-mode instability frequencies of roughly $U_e/(2\delta) \simeq 340$ kHz. These frequencies are too high to be resolved at present. The broad peak near 120kHz may well be first-mode instabilities, but this remains to be clearly demonstrated.

Summary

Purdue University continues to develop the 9.5-inch Boeing/AFOSR Mach-6 Quiet Tunnel, which now provides quiet flow at low Reynolds numbers. A double-wedge centerbody was previously used downstream of the nozzle, both to support the models and to form a second throat. This centerbody caused upstream separation when the nozzle-wall boundary layers became laminar at about 8 psia stagnation pressure. The centerbody has now been removed,

resulting in attached Mach 5.7 quiet flow below 8 psia.

Pitot measurements show that low-noise flow begins at about the same pressure, both halfway down the nozzle and near the nozzle exit. This suggests that transition in the nozzle-wall boundary layer is bypassing the usual linear instability processes, and that the lack of high Reynolds number quiet flow is not due to the very small inflection angle of the present very long nozzle.

Measurements of the static pressure on the diffuser walls show very high fluctuation levels when the nozzle-wall boundary layer is laminar and the bleed-slot flow is entering the diffuser through downstream jets, suggesting the possible importance of the upstream propagation of jet noise from the diffuser. Finally, initial oil-flow images show the development of crossflow vortices on a sharp cones at angle of attack, and initial hot-wire measurements show evidence of instability waves above a sharp cone at zero angle of attack.

Acknowledgements

The research is funded by AFOSR under grant F49620-03-1-0030, by Sandia National Laboratory under contract 80377, and by NASA Langley, under grant NAG1-02047. Partial student support is being provided by Northrop-Grumman. James Kendall (retired from NASA JPL) contributed many helpful suggestions and comments regarding tunnel performance. Scott Berry from NASA Langley contributed to this work while visiting on a Thompson fellowship; the oil-flow measurements in particular use techniques and materials supplied by Langley. Prof. John Sullivan of Purdue suggested the use of tufts. Frank Chen and Steve Wilkinson from NASA Langley continued to provide assistance in making the best possible use of information available from the earlier NASA Langley quiet-tunnel development effort.

REFERENCES

[1] Scott A. Berry, Thomas J. Horvath, Brian R. Hollis, Richard A. Thompson, and H. Harris Hamilton II. X-33 hypersonic boundary layer transition. Paper 99-3560, AIAA, June 1999.

[2] H.A. Korejwo and M.S. Holden. Ground test facilities for aerothermal and aero-optical evaluation of hypersonic interceptors. Paper 92-1074, AIAA, February 1992.

[3] AGARD, editor. *Sustained Hypersonic Flight*. AGARD, April 1997. CP-600, vol. 3.

[4] Tony C. Lin, Wallis R. Grabowsky, and Kevin E. Yelmgren. The search for optimum configurations for re-entry vehicles. *J. of Spacecraft and Rockets*, 21(2):142–149, March-April 1984.

[5] I.E. Beckwith and C.G. Miller III. Aerothermodynamics and transition in high-speed wind tunnels at NASA Langley. *Annual Review of Fluid Mechanics*, 22:419–439, 1990.

[6] Steven P. Schneider. Effects of high-speed tunnel noise on laminar-turbulent transition. *Journal of Spacecraft and Rockets*, 38(3):323–333, May–June 2001.

[7] Steven P. Schneider. Flight data for boundary-layer transition at hypersonic and supersonic speeds. *Journal of Spacecraft and Rockets*, 36(1):8–20, 1999.

[8] S. P. Wilkinson, S. G. Anders, and F.-J. Chen. Status of Langley quiet flow facility developments. Paper 94-2498, AIAA, June 1994.

[9] I. Beckwith, T. Creel, F. Chen, and J. Kendall. Freestream noise and transition measurements on a cone in a Mach-3.5 pilot low-disturbance tunnel. Technical Paper 2180, NASA, 1983.

[10] F.J. Chen, S.P. Wilkinson, and I.E. Beckwith. Görtler instability and hypersonic quiet nozzle design. *J. of Spacecraft and Rockets*, 30(2):170–175, March-April 1993.

[11] Stephen P. Wilkinson. A review of hypersonic boundary layer stability experiments in a quiet Mach 6 wind tunnel. Paper 97-1819, AIAA, June 1997.

[12] S. P. Schneider and C. E. Haven. Quiet-flow Ludwieg tube for high-speed transition research. *AIAA Journal*, 33(4):688–693, April 1995.

[13] J.D. Schmisseur, Steven H. Collicott, and Steven P. Schneider. Laser-generated localized freestream perturbations in supersonic and hypersonic flows. *AIAA Journal*, 38(4):666–671, April 2000.

[14] Terry R. Salyer, Steven H. Collicott, and Steven P. Schneider. Feedback stabilized laser differential interferometry for supersonic blunt body receptivity experiments. Paper 2000-0416, AIAA, January 2000.

[15] Dale W. Ladoon and Steven P. Schneider. Measurements of controlled wave packets at Mach 4 on a cone at angle of attack. Paper 98-0436, AIAA, January 1998.

[16] Steven P. Schneider. Design of a Mach-6 quiet-flow wind-tunnel nozzle using the e**N method for transition estimation. Paper 98-0547, AIAA, January 1998.

[17] Steven P. Schneider, Shin Matsumura, Shann Rufer, Craig Skoch, and Erick Swanson. Progress in the operation of the Boeing/AFOSR Mach-6 quiet tunnel. Paper 2002-3033, AIAA, June 2002.

[18] Steven P. Schneider, Shin Matsumura, Shann Rufer, Craig Skoch, and Erick Swanson. Hypersonic stability and transition experiments on blunt cones and a generic scramjet forebody. Paper 2003-1130, AIAA, January 2003.

[19] Shin Matsumura and Steven P. Schneider. Streamwise-vortex instability and transition on a generic scramjet forebody. Paper 2003-3592, AIAA, June 2003.

[20] Steven P. Schneider. Initial shakedown of the Purdue Mach-6 quiet-flow Ludwieg tube. Paper 2000-2592, AIAA, June 2000.

[21] H. W. Liepmann and A. Roshko. *Elements of Gasdynamics*. John Wiley and Sons, 1957. Republished by Dover, 2002.

[22] Steven P. Schneider. Laminar-flow design for a Mach-6 quiet-flow wind tunnel nozzle. *Current Science*, 79(6):790–799, 25 September 2000.

[23] Steven P. Schneider. Design and fabrication of a 9-inch Mach-6 quiet-flow Ludwieg tube. Paper 98-2511, AIAA, June 1998.

[24] J.C. Sivells. Aerodynamic design of axisymmetric hypersonic wind-tunnel nozzles. *J. Spacecraft*, 7(11):1292–1299, 1970.

[25] R. Benay, B. Chanetz, D. Coponet, Ph. Thobois, and A. Seraudie. Tache 1 du PRF etudes d'ecoulements relatifs a l'avion supersonique: Travaux realises en 2002. Rapport Technique RT 9/06671 DMAE/DAFE, ONERA, Mars 2003. In French. Being translated at Purdue.

[26] Steven P. Schneider and Craig Skoch. Mean flow and noise measurements in the Purdue Mach-6 quiet-flow Ludwieg tube. Paper 2001-2778, AIAA, June 2001.

[27] Steven P. Schneider and Scott E. Munro. Effect of heating on quiet flow in a Mach 4 Ludwieg tube. *AIAA Journal*, 36(5):872–873, May 1998.

[28] Ruth N. Weltmann and Perry W. Kuhns. Heat transfer to cylinders in crossflow in hypersonic rarefied gas streams. Technical Note TN-D-267, NASA, March 1960.

[29] Mark V. Morkovin. Fluctuations and hot-wire anemometry in compressible flows. AGARDograph 24, AGARD, November 1956.

[30] W.S. Saric, H.L. Reed, and E.B. White. Stability and transition of three-dimensional boundary layers. *Annual Review of Fluid Mechanics*, 35:413–440, 2003.

[31] Roger L. Kimmel, Jonathan Poggie, and Stephen N. Schwoerke. Laminar-turbulent transition in a Mach 8 elliptic cone flow. *AIAA Journal*, 37(9):1080–1087, September 1999.

[32] R.L. Kimmel, M.A. Klein, and S.N. Schwoerke. Three-dimensional hypersonic laminar boundary layer computations for transition experiment design. *Journal of Spacecraft and Rockets*, 34(4):409–415, July-August 1997.

[33] W.S. Helliwell and S.C. Lubard. An implicit method for three-dimensional viscous flow with application to cones at angle of attack. Technical Report SAMSO-TR-73-363, Aerospace Corporation, September 1973. DTIC citation AD0770987.

[34] John C. Adams, Jr. Three-dimensional laminar boundary-layer analysis of upwash patterns and entrained vortex formation on sharp cones at angle of attack. Technical Report AEDC-TR-71-215, Arnold Engineering Development Center, December 1971.

[35] John B. McDevitt and Jack A. Mellenthin. Upwash patterns on ablating and nonablating cones at hypersonic speeds. Technical Note TN-D-5346, NASA, July 1969.